Atmos. Meas. Tech. Discuss., 7, 9203–9236, 2014
www.atmos-meas-tech-discuss.net/7/9203/2014/
doi:10.5194/amtd-7-9203-2014
© Author(s) 2014. CC Attribution 3.0 License.

Atmospheric Measurement Techniques Discussions

This discussion paper is/has been under review for the journal Atmospheric Measurement Techniques (AMT). Please refer to the corresponding final paper in AMT if available.

Case study on complex sporadic E layers observed by GPS radio occultations

X. Yue[1], W. S. Schreiner[1], Z. Zeng[1], Y.-H. Kuo[1], and X. Xue[2]

[1]COSMIC Program Office, University Corporation for Atmospheric Research, Boulder, CO, USA
[2]CAS Key Laboratory of Geospace Environment, Department of Geophysics and Planetary Sciences, University of Science and Technology of China, Hefei, Anhui, China

Received: 3 May 2014 – Accepted: 25 August 2014 – Published: 10 September 2014

Correspondence to: X. Yue (xinanyue@ucar.edu)

Published by Copernicus Publications on behalf of the European Geosciences Union.

Abstract

The occurrence of sporadic E (Es) layer has been a hot scientific topic for a long time. Global Navigation Satellite System (GNSS) based Radio Occultation (RO) has been proven a powerful technique on detecting the global Es layers. In this paper, we focus on some cases of complex Es layers based on the RO data from multiple missions processed in UCAR/CDAAC. We first show some examples of multiple Es layers occurred in one RO event. Based on the evaluations between co-located simultaneous RO events and between RO and Lidar observations, it could be concluded that some of these do manifest the multiple Es layered structures. We then show a case of the occurrence of Es in a broad region during a certain time interval. The result is then validated by the independent ionosondes observations. These complex Es structures could be understood well by the popular wind shear theory. We could map the global Es occurrence routinely in the near future given that more RO data will be available. Further statistical studies will enhance our understanding on the Es mechanism. The specification on Es should benefit both the Es based long distance communication and accurate neutral RO retrievals.

1 Introduction

The ionosphere E region is ~ 90–120 km above the Earth's surface. Its electrons mainly origin from the soft X-ray and far ultraviolet (UV) solar radiation ionization of the neutral atmosphere. Regular E region strictly follows the photochemistry equilibrium and therefore could be represented well by a function of the solar zenith angle (Yue et al., 2006). Ionospheric E region has a relatively higher electrical conductivity and therefore plays a crucial role in the ionosphere electron dynamics. The specification of E region could contribute to the studies related to electrojets of high latitude and equatorial region, ionospheric instabilities, and ionosphere-thermosphere-magnetosphere couplings. In addition, it is a key area for long-distance radio communication. Under some certain

AMTD
7, 9203–9236, 2014

circumstances, a thin layer of enhanced ionization would appear in the E region, which is named sporadic E layer (Es). It could be denser than either the E layer peak or even the F layer peak. Es has been investigated extensively both theoretically and experimentally in the past century. It is generally accepted that Es is composed of metallic ions of meteoric origin converged vertically mainly by a wind shear especially in the middle latitude region (Axford, 1963). The wind shear theory has been confirmed by many independent observations and simulations (Haldoupis, 2011; Whitehead, 1989). The occurrence of Es is controlled by multiple factors, including tidal wind, Earth's geomagnetic field, and meteoric deposition of metallic material in the background thermosphere. These factors result in variations of Es occurrence with respect to local time, altitude, latitude, longitude, and season (Haldoupis, 2011). Furthermore, in the high latitude region, the occurrence of Es is more significantly influenced by the local electric field rather than the wind shear due to the geomagnetic field difference (Wakabayashi and Ono, 2005). Please note that the term Es has now been widely used to represent the inhomogeneity of the ionospheric E layer (e.g.: layers, cloud, irregularity, etc.) rather than only the echo trace from ionogram when it was discovered. To learn more about basic Es theory and research progress, the reader can refer to these review papers and the references therein (Haldoupis, 2011; Whitehead, 1989).

Traditionally, Es is mainly observed by the ground-based radars, including Ionosonde and Incoherent/Coherent Scatter Radars (ISR, CSR), and occasional in-situ probes carried by the rockets. Recently, the global navigation satellite system (GNSS) signal based radio occultation (RO) technique has shown great capability in detecting the global Es occurrence by using high resolution Signal to Noise Ratio (SNR) data (Arras et al., 2008; Chu et al., 2014; Hocke et al., 2001; Wu et al., 2005; Yeh et al., 2012; Zeng and Sokolovskiy, 2010). GNSS RO technique has been proven a powerful technique in monitoring climate, weather, and space weather (Anthes, 2011; Foelsche et al., 2011; Liu et al., 2010; Schreiner et al., 2007; Zhang et al., 2011; Yue et al., 2012). After the pioneer GPS/MET mission, many low Earth orbit (LEO) satellites were launched with RO payload, include: CHAMP, GRACE, SAC-C/D, COSMIC, C/NOFS,

AMTD
7, 9203–9236, 2014

Metop-A/B, TerraSAR-X/TanDEM-X, and etc. These observations have accumulated a big database to study the Es. As an example, Fig. 1 shows the altitude variations of the excess phase, relative slant total electron content (TEC) along the LEO-GPS ray, and the SNR during a typical Es event. Due to the occurrence of the Es, both the phase and SNR show simultaneous fluctuations. The SNR has an obvious U-shape as reported by Zeng and Sokolovskiy (2010). The obvious increase of slant TEC around ~ 92 km implies the ionization enhancement in the Es layer. Based on all available GPS/MET RO data, Hocke et al. (2001) did a statistical analysis on the global Es occurrence and compared the results with the Ionosondes observations. Wu et al. (2005) did a more robust statistical analysis on the global Es using CHAMP RO data. The detailed seasonal, latitude, local time, altitude, and hemisphere variations were studied. By combining almost all the available RO data, Arras et al. (2008) showed more fine structure of Es occurrence. Specifically, they gave a direct proof of the control on Es by the Earth's geomagnetic field for the first time and it supported the wind shear theory strongly (Haldoupis, 2011). These statistics are further confirmed by Chu et al. (2014) and Yeh et al. (2012) based on large amount of COSMIC data. Through both simulation and real data analysis, Zeng and Sokolovskiy (2010) revealed that the Es cloud aligned with the wave propagation direction could cause defocusing of the GPS RO signal, accompanied by scintillation above and below the defocusing region due to the interference of direct and refracted radio waves. These effects result in specific U-shape structures in the amplitude of the GPS RO signals. This U-shape will reduce and even disappear with the increase of the tilt angle of the Es cloud with respect to the wave direction. Furthermore, RO amplitude data are also used to detect the high altitude ionospheric irregularity through either back propagation algorithm or analysis on the amplitude variation pattern (Sokolovskiy et al., 2002; Pavelyev et al., 2012; Wickert et al., 2004).

However, some investigations have shown that the Es could be much more complicated than a single layer sometimes. Smith and Miller (1980) used to report the double peaks Es and even a rectangular Es layer observed by rocket. They concluded that the

AMTD
7, 9203–9236, 2014

complex profiles of sporadic-E layers can be interpreted as an effect of unstable wind shears. Based on high resolution ISR observations over Arecibo, Mathews et al. (2001) reported some complex Es layers, which might be due to the modulation of polarized electric field linked with the F region. They reproduced the observed results through 3-D numerical simulations. In addition, some investigations pointed out that the drivers responsible for the plasma instability (e.g.: the Kelvin-Helmholtz Instability (KHI)) could deform the Es layer into a complex structure (Bernhardt, 2002; Cosgrove and Tsunoda, 2003). They could lift up part of the Es layer to overlap with the original layer. Based on the SEEK-2 rocket campaign observations, Wakabayashi and Ono (2005) analyzed the double peaks Es layer phenomena in detail. They found that the lower peak is usually more stable than the upper peak. By using the simultaneous neutral wind and electric field observations, they showed that the neutral wind shear is mainly responsible for the generation of the lower layer, while the DC electric field makes a significant contribution to the formation of the upper layer. However, the complex Es layer can only be observed with the higher vertical resolution technique, such as ISR/CSR and Rocket (Chu and Wang, 1997; Hysell et al., 2012). But there is no corresponding routinely and global distributed observations publicly available, especially the ISR and Rocket, which is not cost effective. According to Haldoupis (2011), the sporadic E layer is actually not sporadic either spatially or temporally. However, it is difficult in the past to identify the Es layer in a broad region simultaneously due to the available sparse ground based observations. The GNSS RO measurements can provide the quasi-vertical profile of ionosphere globally and routinely. It offers us a potential way to study these complex Es layers phenomena.

In this paper, we will conduct some cases studies on multiple Es event observed by COSMIC as well as other missions' atmospheric RO data, which is observed by the occultation antennas of each LEO satellite with ~ 50 Hz resolution. Specifically, two kinds of cases will be investigated. One is multiple Es occurred in a local region observed by one occultation. The other is multiple Es occurrence over a broad region observed by many simultaneously RO events. Multiple Es phenomena have been touched by

AMTD
7, 9203–9236, 2014

some previous studies (Hocke et al., 2001; Yeh et al., 2012). Yeh et al. (2012) even conducted a statistical analysis on the multiple Es layer distribution by ~ 3 years COSMIC RO data. Their results show that the multiple Es layer have almost the similar distribution with respect to geographic location and time as the previous studies by Wu et al. (2005) and Arras et al. (2008). Our study has the following significances in comparison with previous studies. (1) According to Haldoupis (2011), the wind shear below ~ 115 km is dominated by the zonal wind, while it is meridional wind above this altitude, due to the attitudinal variation of the collision frequency between ions and neutrals. This will therefore result in the different time lasting and tidal structures of the Es layers in different altitude. Studies on the multiple Es layers in the same location will be helpful on Es mechanism understanding. (2) As indicated by Zeng and Sokolovskiy (2010), a non-local tilted Es layer could cause the less significant fluctuation of SNR in the lower altitude of the local RO event. It increases difficulty to identify the multiple Es layers by using only one RO event. In this study, we will show how to identify this phenomenon by multiple co-located RO events. (3) We will show how the simultaneously observed RO events in a large broad region enable us to demonstrate that the Es is not sporadic spatially. (4) The bending angle and therefore the refractivity/temperature in the lower atmosphere RO retrievals are influenced significantly by the small scale ionospheric irregularities especially the Es layer (Mannucci et al., 2011). Better understanding of Es in RO signals will benefit the improvement of neutral atmosphere retrievals and therefore the numerical weather prediction (NWP) and climate change study.

The remainder of the paper is organized as follows. Section 2 shows the examples of multiple peaks Es layers in the same location. The example of Es occurred in a broad region simultaneously observed by multiple RO events is given in Sect. 3. We then discuss and conclude in Sects. 4 and 5, respectively.

AMTD
7, 9203–9236, 2014

2 Case study 1: multiple peaks Es layer in the same location

The identification of Es occurrence is different from paper to paper (Arras et al., 2008; Chu et al., 2014; Dou et al., 2010; Hocke et al., 2001; Wu et al., 2005; Yeh et al., 2012; Zeng and Sokolovskiy, 2010). Hocke et al. (2001) and Dou et al. (2010) derived the Es occurrence from the fluctuations of RO inverted electron density profiles. Wu et al. (2005) and Arras et al. (2008) calculated the standard deviation of filtered and normalized SNR and identified the Es occurrence through either the maximum standard deviation or a threshold. Chu et al. (2014) applied a more critical criteria on both the amplitude and phase fluctuations of L1 and L2 signals to avoid the potential influences from the instrument and measurement noise. In this study, only the cases that have maximum S4 index calculated from 50 Hz SNR larger 0.3 are considered. The Es occurrence will then be identified manually from case to case. Only the case that show visible fluctuations of L1/2 SNR and phases and obvious enhancement of slant TEC around the E region will be considered.

2.1 Multiple peaks Es examples

As stated, the Es layer can cause the defocusing and scintillation of the SNR of RO signals. So the Es occurrence can be identified from the fluctuation of the SNR. In the mean time, the enhanced ionization in Es layer also results in additional phase delay of the radio signal and therefore the enhancement of the slant TEC along the GNSS ray. When we looked at the RO data case by case, we can find many cases that have more then one peaks in SNR or slant TEC along the tangent height. We give 3 typical such examples in Fig. 2. The case in Fig. 2a was observed by COSMIC satellite FM4 during 2013.183. Both SNR fluctuation and slant TEC show a major and minor peaks around ~ 105 and 93 km, respectively. In Fig. 2b case, the SNR/TEC shows one larger peak around ~ 100 km and two smaller peaks around 84 and 67 km, respectively. Figure 2c shows an extreme case with up to seven visible peaks in both SNR fluctuation and slant TEC. Please note that the much larger range of TEC amplitude here makes

AMTD
7, 9203–9236, 2014

its enhancements less visible, although the TEC peaks are actually significant in this case. Due to the special observational geometry of RO, either the SNR or the slant TEC actually reflects the integral effect along the whole GNSS ray. When we assign these values to the tangent points of the GNSS ray, the effect of the Es layer in the higher altitude could map down to the lower tangent point altitude, which might result in pseudo multiple peaks along the tangent points altitude, as shown in Fig. 2 (Zeng and Sokolovskiy, 2010). However, the Es layer mostly extends horizontally. For a specific GNSS ray, the effect of Es far from the tangent points will be much smaller than that of Es in the tangent points area due to the tilt angle between Es layer and GNSS ray. In the following, we will show two kinds of validation studies on the multiple Es peaks in the same RO event.

2.2 Evaluation by co-located simultaneous RO events

In the University Corporation for Atmospheric Research (UCAR) COSMIC Data Analysis and Archive Center (CDAAC), we process most available RO data for the community (Schreiner et al., 2011). These missions include COSMIC, CHAMP, GRACE, SACC, TerraSAR-X, C/NOFS, and MetopA/B. These combined missions can generate 3000–4000 RO events daily in terms of atmospheric excess phase (atmPhs). This number varies with time due to either satellite lunching or degradation. One potential way to evaluate the multiple Es layers is looking at the co-located RO events. If two co-located RO events with totally different azimuth angles show the similar multiple Es structures at the same time, we can conclude that these structures are the realistic structures. We searched the co-located RO events among all CDAAC data during 2012–2013. The Metop data is excluded because it begins to sample the occultation around ~ 80 km altitude usually. The co-location criteria is that the difference of latitude, longitude, and universal time in 100 km altitude of the tangent point between two occultations is less than 1°, 2°, and 15 min, respectively. This criterion is far smaller than the typical spatial and temporal scales of Es. In addition, the azimuth angle difference between two occultations in 100 km altitude should be larger than 60°, to ensure that the

AMTD
7, 9203–9236, 2014

areas away from the tangent points of two occultations have no overlap. Those short occultations having no integral coverage of 90–120 km will be discarded too. The excess phase, SNR, and relative slant TEC of these co-located occultations were printed out to be further checked manually. Generally, we can find ~ 6–10 co-located RO pairs per day on average. Unfortunately, some of them either have no Es occurrence or only one peak Es, which is beyond the focus of this study. Finally, we found ~ 100 cases manually that both co-located occultations show visible double peaks in both SNR and slant TEC at the same tangent point altitude. Since two occultations sample the totally different area and intersect with each other in the tangent point area, there is a high possibility that these double peak Es layers are the realistic double Es layers occurred around the tangent points area. As examples, we show two such cases in Figs. 3 and 4, respectively. In Fig. 3, two occultations made by COSMIC FM5-GPS31 and FM2-GPS23 within 2 min around the southern middle latitude during 2012.044 local sunset time are displayed. Indicated from the SNR and TEC variations, two Es layers around 114 and 95 km occurred simultaneously in two occultations. In another case shown in Fig. 4, two simultaneous occultations made by FM6-GPS15 and FM2-GPS11 around southern middle-latitude area local afternoon time are shown. One major peak around 113 km and another minor peak around 92 km can be identified in both occultations. The SNR around two peaks have obvious U-shape, which indicates that the tilt angle between Es direction and GPS ray is insignificant (Zeng and Sokolovkiy, 2010).

2.3 Independent evaluation by Lidar observations

According to Gardner et al. (1993), sporadic metal (Fe and Na) layers could be observed simultaneously with the sporadic E layer due to the neutralization of metal ions (Fe^+ and Na^+) in the associated Es layer. Dou et al. (2010) have compared the Es derived from COSMIC electron density profiles with the meteors from a meteor radar and the sodium atom layers from a Lidar statistically. Well correlated seasonal variations were detected among three parameters. It implies the linkage between multiple Es and metal layers. Another potential way to evaluate these multiple peaks Es layers is by

AMTD
7, 9203–9236, 2014

comparing with the Lidar results. In this study, the Lidar observations made in Beijing (40.2° N, 116.2° E), Hefei (31.8° N, 117.3° E), Wuhan (30.5° N, 114.4° E), and Haikou (19.5° N, 109.1° E) over China accessed from the Chinese Meridian Project during 2012 are used (Wang, 2011). Detailed information about these Lidar stations can be found in Dou et al. (2013). Based on these Lidar observations, Dou et al. (2013) have done some statistical investigations on the occurrence of sporadic sodium layers (SSLs) and the thermosphere enhanced sodium layers (TeSLs) in China during 2011–2012. The TeSLs is defined as the secondary sodium layer in the lower thermosphere separated from the main SSLs (Dou et al., 2013). We are not going to look at the whole Lidar observations in this study. Instead, we tried to search the COSMIC RO events nearby the Lidar stations for the TeSLs cases listed in the table A2 of Dou et al. (2013). These TeSLs were all observed during local nighttime and the lasting time ranges from ∼ 1 h up to ∼ 6 h. The co-location criteria is that the difference of latitude and longitude between Lidar and RO tangent points at the altitude of 100 km is less than 2.5° and 4.5°, respectively, and the occurrence time of RO is within the TeSLs occurrence. Of all 28 cases, we finally found a perfect case during 29 July 2012 (DOY: 211) over HaiKou Lidar station. Before showing the results of this case, we would like to define a concept called the Es Occurrence Area (EOA) for convenience. As shown in Fig. 5, the peaks of either SNR or TEC in tangent point C could only origin from the Es layers located above that altitude along the BB' GNSS ray. Usually, the Es layer occurs in the altitude range of 85–130 km (Haldoupis, 2011). We do not consider the intermediate layer because most RO missions were designed to make the high resolution sampling around 130 km (Arras et al., 2009; Li et al., 2013). So the Es layers in the plots could only come from the area between 85 and 130 km that the GNSS rays passing through. This area is defined as the Es Occurrence Area (EOA), as shown by the shadow area in Fig. 5. In the 29 July 2012 TeSLs case over Haikou Lidar station, the TeSLs begins to separate from the main SSL around ∼ 15:00 (UT), becomes distinguishable at 15:32, peaks around 16:00 at 113 km altitude, and ends at 18:19. During the whole TeSLs occurrence interval, there exist significant SSLs with peaks around ∼ 93 km. There are

AMTD
7, 9203–9236, 2014

totally 4 COSMIC co-located ROs observed at 15:20, 15:30, 15:50, and 16:03 UT, respectively. The first two ROs are made by COSMIC FM2 and occurred in the initial phase of TeSLs, while the latter two are by FM1 around the peak of TeSLs. Figure 6 shows the geo-location of the Hai Kou Lidar station and the EOA of the four co-located RO events. The EOA of four RO have few overlaps, which imply that the observed Es by the RO events are independent. The SNR/TEC of RO events and the Na density of Hai Kou Lidar corresponding to the RO occurrence time are given in Fig. 7. As indicated from the altitude variations of the SNR/TEC, all 4 RO events show obvious complex Es occurrence. In case 1, the occultation is along the southwest-northeast direction and flit over the Hai Kou lidar station. The SNR/TEC show simultaneous fluctuations at the altitude range of 85–110 km. While in case 2, the RO event is ~ 500 km west of Hai Kou and the SNR/TEC fluctuate in almost all the altitudes. In both cases, the SNR oscillations are not constant and show some minor peaks occasionally. It excludes the potential effects from the F region ionospheric scintillations (Straus et al., 2003). During the occurrence of cases 1 and 2, the TeSLs is separating from the main SSL. Since the TeSLs is mainly formed from the neutralization of the metal ions, the ionosphere might experience complicated dynamic and chemistry evolutions during the initial phase of TeSLs. RO measurements confirmed that the ionization are complicated and no distinct layered structures are formed at that time, which is consistent with the Na density observations. In cases 3 and 4, the TeSLs are already distinguishable. Both RO events show two peaks in ~ 100 and 108 km, respectively, in terms of either SNR or slant TEC. In case 3, the higher altitude peak is smaller than the lower peak, while the situation is reversed in case 4. This might be caused by the different geometry of occultation, which result in the difference of the tilt angle between Es and GNSS ray. Please note the peak altitude and amplitude between RO and Lidar observations are not necessarily consistent due to the different dynamic processes therein. The Na density used here is mainly to demonstrate the potential existence of multiple Es layer in the ionosphere which is confirmed by the RO measurements.

AMTD
7, 9203–9236, 2014

3 Case study 2: multiple simultaneous Es layer in a broad region

Es was mainly observed by the ionosondes at the beginning stage. The Es can only be identified by ionosonde when larger than a certain value because most ionosonde transmitters have a low limitation on the transmitted wave frequency (~ 1–1.5 MHz). It makes the appearance of Es "sporadic" vs. space and time (Haldoupis, 2011). However, the wind shear theory suggests that Es is closely linked to the atmospheric dynamics. Inherently, this implies that Es possesses a variable but regular character that reflects both, the complexity and repeatability of the atmospheric wind and wave dynamics in the mesosphere-lower thermosphere (MLT) region. The high resolution and sensitivity observations made by ISR in Arecibo have confirmed that Es is present all times in some cases, which exhibits a non-sporadic behavior (Mathews, 1998). Mathews (1998) even proposed an alternative term "tidal ion layers (TIL)" because "sporadic" is an instrumental limitation rather than a prominent physical property (Haldoupis, 2011). The ISR observations already prove the non-sporadic property of Es with respect to time. However, due to the lack of global Es observations, there is still no direct evidence to prove that Es is also non-sporadic spatially in the past. The global distribution feature of RO technique enables us to find direct evidence for the first time.

Although we can observe 3000–4000 RO events daily and globally by the combined multiple RO missions, it is still impossible to get enough occultations in a certain time and space range. Fortunately, right after the launch, the six COSMIC satellites were clustered together in one orbit and the distances between LEOs increased gradually (Schreiner et al., 2007). It enables tracking multiple RO events in a broad region simultaneously in the certain stage of LEO orbit separation. We looked through all the COSMIC RO data as well as occultations available from other missions during 2006. Finally, we found many cases that multiple LEOs sample a certain region in a certain time. Part of these cases show that the Es do can occur in a broad region simultaneously, which support that Es is non-sporadic spatially too. Those cases are mainly found in the middle latitude of Eurasian continent and pacific ocean. This is understandable

AMTD
7, 9203–9236, 2014

because the relative higher horizontal component of geomagnetic field over this region makes the wind shear more efficient (Haldoupis, 2011). To evaluate these results, the raw ionograms accessed from the Digital Ionogram DataBase (DIDB) operated by the Lowell Global Ionospheric Radio Observatory (GIRO) Data Center (LGDC) through the SAO Explorer software are used to make independent comparison (Galkin et al., 1999; Reinisch and Galkin, 2011). During 2006, there are totally about 35–40 ionosonde stations sharing their data in DIDB. Generally, the Europe and northern America have relatively more and denser ionosondes distribution. We checked the ionograms over these regions during the occurrence of simultaneous Es over a broad region indicated by RO. For most cases, we can find the visible Es occurrence in the corresponding ionograms. Figures 8–11 show such an example over the Europe region.

During 2006.294 (21 October), except FM5, which was already raised to a higher orbit, the rest 5 satellites of COSMIC have adjacent orbits. FM3 and FM4 even have almost the same orbit within 200 km distance. There are totally 62 RO events observed over $10^{\circ} \sim 60^{\circ}$ latitude and $-20^{\circ} \sim 45^{\circ}$ longitude area during 11:00–15:00 UT interval. Through our manually checking, 50 of them show obvious Es related oscillations in SNR. Figure 8 shows the LEOs' orbits and these 50 RO events. The EOA is again shown here for each occultation to demonstrate the independence of the observed Es between different ROs. Each occultation is labeled by an index number ($1 \sim 50$). The corresponding altitude variations of SNR are shown in Fig. 9. Note that the SNR is normalized to the range of 0–1 for the convenience. As indicated from the figure, All the ROs selected here show obvious oscillations related to Es. Most of the SNRs have a visible U-shape, which illustrates that the Es is significant. At this specific region and time interval, the DIDB has 7 ionosondes that have observations available. The geolocation, ionosondes system type, and the operation organization are given in Table 1. The red stars in Fig. 8 represent the geographic distribution of the ionosondes. The hourly ionograms of 7 ionosondes during 11:00–15:00 UT are plotted in Fig. 10, with emphasize on the wave traces below 150 km by black dots. We can see clearly the wave traces due to the Es in most ionograms except in 11:00 UT and 12:00 UT of

AMTD
7, 9203–9236, 2014

Athens. Please note the different noise level between the ionograms by different types of ionosondes. In Fig. 11, we plotted the automatic scaled Es critical frequency (foEs) and the E layer critical frequency (foE) of 7 ionosondes, and the averaged IRI modeled foE vs. local time (Bilitza and Reinisch, 2008). The high occurrence rate of Es can be identified. Although these 7 ionosondes distribute in a relative narrow area, they still strongly support the simultaneous occurrence of Es over a broad region.

4 Discussions

4.1 Multiple Es layers in one profile

We have summarized some complex Es layers observed by rockets and ISRs from previous publications (Smith and Miller, 1980; Mathews et al., 2011; Bernhardt, 2002; Cosgrove and Tsunoda, 2003; Wakabayashi and Ono, 2005). In Sect. 2, we reported some examples of RO events that show multiple peaks in the tangent altitude variations of either SNR or relative slant TEC, which manifest the potential complex multiple layered structures of Es in the occultation area. Then we showed some double peaks Es layers observed by simultaneously co-located RO events with different azimuth angles to prove that these double peaks Es layers are not probably caused by the localization problem and could be realistic. Furthermore, we also gave an example of comparison between the complex Es layers made by 4 RO events and the co-located Lidar observed double sporadic Na layers (TeSLs). With the time evolving of TeSLs, RO measurements show complex Es accordingly. Actually, Xue et al. (2013) also reported an example showing that the Lidar observes TeSLs associated with simultaneous double peaks of SNR made by co-located RO event from TerraSAR-X. According to wind shear theory, at lower (upper) altitude, the zonal (meridional) wind will dominate the shear due to the altitude variations of the ion-neutral collision frequency to the ion gyro-frequency ratio. In comparison with the low altitude, the Es layers in the upper altitude are more variable and short-lived since ion-convergence is much faster there

AMTD
7, 9203–9236, 2014

(Haldoupis, 2011). Similarly, an existing Es layer could be broadened and dissipated by an opposite wind shear. The layers can deform faster (slower) at the altitudes where they form faster (slower). This is the reason why Es layers remain fairly stable for many hours at lower heights, while much shorter in the high altitude. The Es is controlled by the tidal wind and therefore shows also tidal structures in their formation and descent. Main tidal components include diurnal, semi-diurnal, and even terdiurnal and quarter-diurnal (Arras et al., 2009; Chu et al., 2014; Fytterer et al., 2013; Wu et al., 2005). All these factors make the complex Es layer structures understandable. However, due to the limited amount of data availability from ISR and rockets, the investigations on this issue were mainly made through either theoretical analysis or case study. The huge amount of accumulated RO events enable us to study this phenomena statistically, which will be done in a further study. This kind of investigation will definitely enhance our understanding on the Es mechanism.

4.2 Es occurrence simultaneously in a broad region

We have found many cases that show simultaneous Es occurrence over a broad region made by clustered COSMIC satellites in the early stage. One of these cases is displayed in the paper and evaluated by the independent ionosondes observations. Regarding this comparison, we should be aware of two key points. (1) In the RO SNR profile, we can see that some cases show the Es occurrence below even 80 km. However, due to the localization problem of RO geometry as stated above, these Es could either happen in that altitude of the tangent point or in a higher altitude of beyond tangent point due to mapping effect along the GNSS ray. If the Es occurs below 80 km, it could not be resulted from the wind shear theory because of the high collision frequency between ionization and neutral particles over the lower altitude. (2) According to Whitehead (1989), the thickness of Es is usually less than 4 km. As indicated from Fig. 10, sometimes the vertical extent of echo trace can be larger than 10 km. This might have additional drivers beyond Es. The echo trace in ionogram could have a variety of sources (Maruyama et al., 2006). But we are sure that these irregularities,

AMTD
7, 9203–9236, 2014

which can cause echo traces in ionogram, will cause the RO SNR fluctuations too if the horizontal extent is sufficiently long.

We have not seen any such cases of broad Es occurrence report in the previous literature. One reason is that the available Es observations from global ionosondes and CSR/ISRs are still far less than enough coverage to study this phenomena. Another reason is that the mainly used ionosondes have lower frequency limitation, as we stated before. Opposite from that, the high resolution RO radio wave signal is very sensitivity to the layered structure in the ionosphere, which has been proved by the simulation studies by Yeh et al. (2012) and Zeng and Sokolovskiy (2010). During that selected case, the ionosphere is geomagnetically quiet (minimum dst index is −28 nT). We can exclude the potential effects from the storm time penetration electric field, which can result in broad region Es occurrence as reported by some studies (Abdu et al., 2014). The region of simultaneous occurrence of Es is roughly 50° width (10° ∼ 60°) in latitude and 65° width (−20° ∼ 45°) in longitude. We actually have found some other cases, which show quasi simultaneous Es occurrence in a much larger area especially in east Asia region. It is not selected to be shown here because fewer co-located ionosondes are available to do the evaluation over there. Our results strongly support the non-sporadic property of Es, as proposed by Haldoupis (2011) and Mathews (1998). However, current RO observations are still far less than sufficient to map the global Es in anytime. In the near future, with the dramatic increase of available RO events from different planned RO missions (*Status of the global Radio Occultation Observing System, CGMS-40 EUM-WP-02:* http://irowg.org/wpcms/wp-content/uploads/2013/12/Status_of_the_global_Radio_Occultation_observing_system.pdf), it will enable us to map the global Es occurrence routinely. It will benefit the Es research as well as some applications such as the long-distance communication at VHF frequencies via reflections from Es layers.

AMTD
7, 9203–9236, 2014

4.3 Wind shear theory

Yeh et al. (2012) and Chu et al. (2014) have examined the winder shear theory based on RO Es occurrence in very detail. In Chu et al. (2014), they compared the COSMIC Es global morphology with the parameters that control the wind shear, including the global horizontal magnetic field intensity, global Fe^+ distribution from the WACCM model calculation (Feng et al., 2013), and the meridional and zonal winds from HWM model. Based on these parameters, they also calculated the global distribution of the divergence of the vertical Fe^+ flux. According to their results, the wind shear can explain the global distribution of Es and their altitude, local time, seasonal, and hemispheric asymmetry quite well especially in middle latitude. The tidal wind and geomagnetic field are quite stable. According to Feng et al. (2013), the Fe^+ density is also substantial distributed globally. We can conclude that the simultaneously occurrence of Es in a broad region under wind shear theory is possible. The case 2 therefore supports the wind shear theory. It also demonstrates the advantages of RO signals in terms of high sensitive to the sporadic E occurrence.

5 Conclusions

In this case study, the high resolution GNSS RO signals from multiple missions processed in UCAR/CDAAC are used to investigate the complex Es layer structures. The selected cases are evaluated by co-located simultaneous RO events and independent observations from Lidar and ionograms. We got the following key points:

1. The Es occurrence could be identified by either the relative slant TEC peak or the SNR fluctuations (or U-shape sometimes) from the RO measurements.

2. Only the Es from the defined Es Occurrence Area (EOA) can result in Es related features in a RO event.

AMTD
7, 9203–9236, 2014

3. When assigning the observations to the tangent height, either SNR or TEC might show multiple Es layers structures. Based on the evaluations between co-located simultaneous RO events and between RO and lidar observations, we conclude that some of these do manifest the multiple Es layered structures.

4. We have found some cases that show the occurrence of Es in a broad region during a certain time interval. The result is then validated by the independent ionosondes observations.

5. These complex Es structures could be understood well by the popular wind shear theory. Further studies could benefit both the Es mechanism research and relevant applications.

Acknowledgements. This material is based upon work supported by the National Science Foundation under Cooperative Agreement AGS-1033112. X. Xue acknowledges the support by the Project (KJCX2-EW-J01) of Chinese Academy of Science. We acknowledge the usage of the Lidar data from the Chinese Meridian Project and the ionosonde data accessed through the Lowell Global Ionospheric Radio Observatory (GIRO) Data Center (LGDC) Digital Ionogram DataBase (DIDB). We appreciate the organizations presented in Table 1 for making their Ionosondes observations publicly available.

References

Abdu, M. A., de Souza, J. R., Batista, I. S., Santos, A. M., Sobral, J. H. A., Rastogi, R. G., and Chandra, H.: The role of electric fields in sporadic E layer formation over low latitudes under quiet and magnetic storm conditions, J. Atmos. Sol.-Terr. Phys., 115–116, 95–105, doi:10.1016/j.jastp.2013.12.003, 2014.

Anthes, R. A.: Exploring Earth's atmosphere with radio occultation: contributions to weather, climate and space weather, Atmos. Meas. Tech., 4, 1077–1103, doi:10.5194/amt-4-1077-2011, 2011.

Arras, C., Wickert, J., Beyerle, G., Heise, S., Schmidt, T., and Jacobi, C.: A global climatology of ionospheric irregularities derived from GPS radio occultation, Geophys. Res. Lett., 35, L14809, doi:10.1029/2008GL034158, 2008.

AMTD

7, 9203–9236, 2014

Arras, C., Jacobi, C., and Wickert, J.: Semidiurnal tidal signature in sporadic E occurrence rates derived from GPS radio occultation measurements at higher midlatitudes, Ann. Geophys., 27, 2555–2563, doi:10.5194/angeo-27-2555-2009, 2009.

Axford, W. I.: The formation and vertical movement of dense ionized layers in the ionosphere due to neutral wind shears, J. Geophys. Res., 68, 769–779, 1963.

Bernhardt, P. A.: The modulation of sporadic-E layers by Kelvin–Helmholtz billows in the neutral atmosphere, J. Atmos. Sol.-Terr. Phys., 64, 1487–1504, 2002.

Bilitza, D. and Reinisch, B. W.: International reference ionosphere 2007: improvements and new parameters, Adv. Space Res., 42, 599–609, doi:10.1016/j.asr.2007.07.048, 2008.

Chu, Y. H. and Wang, C. Y.: Interferometry observations of three-dimensional spatial structures of sporadic E irregularities using the Chung-Li VHF radar, Radio Sci., 32, 817–832, 1997.

Chu, Y. H., Wang, C. Y., Wu, K. H., Chen, K. T., Tzeng, K. J., Su, C. L., Feng, W., and Plane, J. M. C.: Morphology of sporadic E layer retrieved from COSMIC GPS radio occultation measurements: Wind shear theory examination, J. Geophys. Res, 119, 2117–2136, doi:10.1002/2013JA019437, 2014.

Cosgrove, R. B. and Tsunoda, R. T.: Simulation of the nonlinear evolution of the sporadic-E layer instability in the nighttime midlatitude ionosphere, J. Geophys. Res., 108, 1283, doi:10.1029/2002JA009728, 2003.

Dou, X.-K., Xue, X. H., Li, T., Chen, T. D., Chen, C., and Qiu, S.-C.: Possible relations between meteors, enhanced electron density layers, and sporadic sodium layers, J. Geophys. Res., 115, A06311, doi:10.1029/2009JA014575, 2010.

Dou, X. K., Qiu, S. C., Xue, X. H., Chen, T. D., and Ning, B. Q.: Sporadic and thermospheric enhanced sodium layers observed by a lidar chain over China, J. Geophys. Res., 118, 6627–6643, doi:10.1002/jgra.50579, 2013.

Foelsche, U., Scherllin-Pirscher, B., Ladstädter, F., Steiner, A. K., and Kirchengast, G.: Refractivity and temperature climate records from multiple radio occultation satellites consistent within 0.05 %, Atmos. Meas. Tech., 4, 2007–2018, doi:10.5194/amt-4-2007-2011, 2011.

Hysell, D. L., Nossa, E., Larsen, M. F., Munro, J., Smith, S., Sulzer, M. P., and González, S. A.: Dynamic instability in the lower thermosphere inferred from irregular sporadic E layers, J. Geophys. Res., 117, A08305, doi:10.1029/2012JA017910, 2012.

Feng, W., Marsh, D. R., Chipperfield, M. P., Janches, D., Hoffner, J., Yi, F., and Plane, J. M. C.: A global atmospheric model of meteoric iron, J. Geophys. Res.-Atmos., 118, 9456–9474, doi:10.1002/jgrd.50708, 2013.

AMTD
7, 9203–9236, 2014

Fytterer, T., Arras, C., and Jacobi, C.: Terdiurnal signatures in sporadic *E* layers at midlatitudes, Adv. Radio Sci., 11, 333–339, doi:10.5194/ars-11-333-2013, 2013.
Galkin, I. A., Kitrosser, D. F., Kecic, Z., and Reinisch, B. W.: Internet access to ionosondes, J. Atmos. Sol.-Terr. Phy. 61, 181–186, 1999.
Gardner, C. S., Kane, T. J., Senft, D. C., Qian, J., and Papen, G. C.: Simultaneous observations of sporadic E, Na, Fe, and Ca^+ layers at Urbana, Illinois: three case studies, J. Geophys. Res., 98, 16865–16873, doi:10.1029/93JD01477, 1993.
Haldoupis, C.: A Tutorial Review on Sporadic E Layers, Aeronomy of the Earth's Atmosphere and Ionosphere, IAGA Special Sopron Book Series 2, 381–394, 2011.
Hocke, K., Igarashi, K., Nakamura, M., Wilkinson, P., Wu, J., Pavelyev, A., and Wikert, J.: Global sounding of sporadic E layers by the GPS/MET radio occultation experiment, J. Atmos. Sol.-Terr. Phys., 63, 1973–1980, doi:10.1016/S1364-6826(01)00063-3, 2001.
Li, G., Ning, B., Patra, A. K., Abdu, M. A., Chen, J., Liu, L., and Hu, L.: On the linkage of daytime 150 km echoes and abnormal intermediate layer traces over Sanya, J. Geophys. Res., 118, 7262–7267, doi:10.1002/2013JA019462, 2013.
Liu, J. Y., Lin, C. Y., Lin, C. H., Tsai, H. F., Solomon, S. C., Sun, Y. Y., Lee, I. T., Schreiner, W. S., and Kuo, Y. H.: Artificial plasma cave in the low-latitude ionosphere results from the radio occultation inversion of the FORMOSAT-3/COSMIC, J. Geophys. Res., 115, A07319, doi:10.1029/2009JA015079, 2010.
Mannucci, A. J., Ao, C. O., Pi, X., and Iijima, B. A.: The impact of large scale ionospheric structure on radio occultation retrievals, Atmos. Meas. Tech., 4, 2837–2850, doi:10.5194/amt-4-2837-2011, 2011.
Maruyama, T., Saito, S., Yamamoto, M., and Fukao, S.: Simultaneous observation of sporadic E with a rapid-run ionosonde and VHF coherent backscatter radar, Ann. Geophys., 24, 153–162, doi:10.5194/angeo-24-153-2006, 2006.
Mathews, J. D.: Sporadic E: current views and recent progress, J. Atmos. Sol.-Terr. Phys., 60, 413–435, 1998.
Mathews, J. D., Machuga, D. W., and Zhou, Q.: Evidence for electrodynamic linkages between spread-F, ion rain, the intermediate layer, and sporadic E: results from observations and simulations, J. Atmos. Sol.-Terr. Phys., 63, 1529–1543, 2001.
Pavelyev, A. G., Liou, Y. A., Zhang, K., Wang, C. S., Wickert, J., Schmidt, T., Gubenko, V. N., Pavelyev, A. A., and Kuleshov, Y.: Identification and localization of layers in the ionosphere

AMTD
7, 9203–9236, 2014

using the eikonal and amplitude of radio occultation signals, Atmos. Meas. Tech., 5, 1–16, doi:10.5194/amt-5-1-2012, 2012.
Reinisch, B. W. and Galkin, I. A.: Global ionospheric radio observatory (GIRO), Earth Planets Space , 63, 377–381, doi:10.5047/eps.2011.03.001, 2011.
Schreiner, W., Rocken, C., Sokolovskiy, S., Syndergaard, S., and Hunt, D.: Estimates of the precision of GPS radio occultations from the COSMIC/FORMOSAT-3 mission, Geophys. Res. Lett., 34, L04808, doi:10.1029/2006GL027557, 2007.
Schreiner, W., Sokolovskiy, S., Hunt, D., Rocken, C., and Kuo, Y.-H.: Analysis of GPS radio occultation data from the FORMOSAT-3/COSMIC and Metop/GRAS missions at CDAAC, Atmos. Meas. Tech., 4, 2255–2272, doi:10.5194/amt-4-2255-2011, 2011.
Smith, L. G. and Miller, K. L.: Sporadic-E layers and unstable wind shears, J. Atmos. Terr. Phys., 42, 45–50, 1980.
Sokolovskiy, S., Schreiner, W., Rocken, C., and Hunt, D.: Detection of high-altitude ionospheric irregularities with GPS/MET, Geophys. Res. Lett., 29, 1033, doi:10.1029/2001GL013398, 2002.
Straus, P. R., Anderson, P. C., and Danaher, J. E.: GPS occultation sensor observations of ionospheric scintillation, Geophys. Res. Lett., 30, 1436, doi:10.1029/2002GL016503, 2003.
Wakabayashi, M. and Ono, T.: Multi-layer structure of mid-latitude sporadic-*E* observed during the SEEK-2 campaign, Ann. Geophys., 23, 2347–2355, doi:10.5194/angeo-23-2347-2005, 2005.
Wang, C.: New chains of space weather monitoring stations in China, Space Weather, 8, S08001, doi:10.1029/2010SW000603, 2011.
Whitehead, J. D.: Recent work on midlatitude and equatorial sporadic E, J. Atmos. Terr. Phys., 51, 401–424, 1989.
Wickert, J., Pavelyev, A. G., Liou, Y. A., Schmidt, T., Reigber, C., Igarashi, K., Pavelyev, A. A., and Matyugov, S.: Amplitude variations in GPS signals as possible indicator of ionospheric structures, Geophys. Res. Lett., 31, L24801, doi:10.1029/2004GL020607, 2004.
Wu, D. L., Ao, C. O., Hajj, G. A., Torre Juarez, M. de la, and Mannucci, A. J.: Sporadic E morphology from GPS-CHAMP radio occultation, J. Geophys. Res., 110, A01306, doi:10.1029/2004JA010701, 2005.
Xue, X. H., Dou, X. K., Lei, J., Chen, J. S., Ding, Z. H., Li, T., Gao, Q., Tang, W. W., Cheng, X. W., and Wei, K.: Lower thermospheric enhanced sodium layers observed at low latitude and pos-

AMTD
7, 9203–9236, 2014

sible formation: case studies, J. Geophys. Res., 118, 2409–2418, doi:10.1002/jgra.50200, 2013.
Yeh, W.-H., Huang, C.-Y., Hsiao, T.-Y., Chiu, T.-C., Lin, C.-H., and Liou, Y.-A.: Amplitude morphology of GPS radio occultation data for sporadic-E layers, J. Geophys. Res., 117, A11304, doi:10.1029/2012JA017875, 2012.
Yue, X., Wan, W., Liu, L., and Ning. B.: An empirical model of ionospheric foE over Wuhan, Earth Planets Space, 58, 323–330, 2006.
Yue, X., Schreiner, W. S., Kuo, Y.-H., Hunt, D. C., Wang, W., Solomon, S. C., Burns, A. G., Bilitza, D., Liu, J.-Y., Wan, W., and Wickert, J.: Global 3-D ionospheric electron density reanalysis based on multi-source data assimilation, J. Geophys. Res., 117, A09325, doi:10.1029/2012JA017968, 2012.
Zeng, Z. and Sokolovskiy, S.: Effect of sporadic E cloud on GPS radio occultation signal, Geophys. Res. Lett., 37, L18817, doi:10.1029/2010GL044561, 2010.
Zhang, K., Fu, E., Silcock, D., Wang, Y., and Kuleshov, Y.: An investigation of atmospheric temperature profiles in the Australian region using collocated GPS radio occultation and radiosonde data, Atmos. Meas. Tech., 4, 2087–2092, doi:10.5194/amt-4-2087-2011, 2011.

AMTD
7, 9203–9236, 2014

Table 1. Latitude, longitude, ionosonde system type, and operation organization/country of the 7 used ionosondes in the study. DGS-256: Digisonde-256; DPS-1: Single-Receiver Digisonde Portable Sounder; DPS-4: Four-Receiver Digisonde Portable Sounder.

Station	latitude	longitude	Ionosonde	Organization/Country
Athens	38.0° N	23.5° E	DPS-4	National Observatory of Athens, Greece
Dourbes	50.1° N	4.6° E	DGS-256	Royal Meteorological Institute, Belgium
Roquetes	40.8° N	0.3° E	DGS-256	Observatori de l'Ebre, Spain
Juliusruh	54.6° N	13.4° E	DPS-1	Institute of Atmospheric Research, University of Rostock, Germany
Pruhonice	50.0° N	14.6° E	DPS-4	Institute of Atmospheric Physics, Czech Republic
Chilton	51.5° N	0.6° W	DPS-1	Rutherford Appleton Laboratory, UK
Rome	41.9° N	12.5° E	DPS-4	L'Instituto Nazionale di Geofisica, Italy

AMTD
7, 9203–9236, 2014

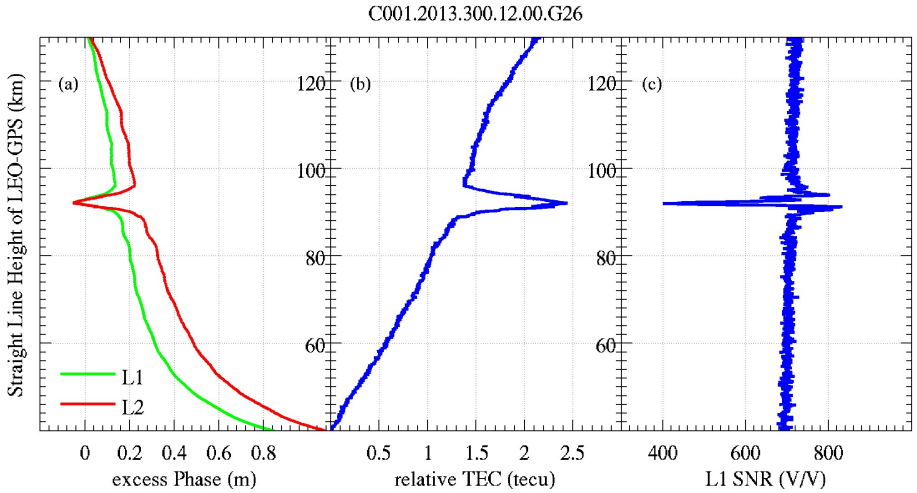

Figure 1. Straight line height variations of excess Phase **(a)**, relative slant TEC **(b)**, and L1 SNR **(c)** of one selected radio occultation event observed by COSMIC FM1 during 2013.300 when there is a sporadic E layer occurrence over the occultation region.

AMTD
7, 9203–9236, 2014

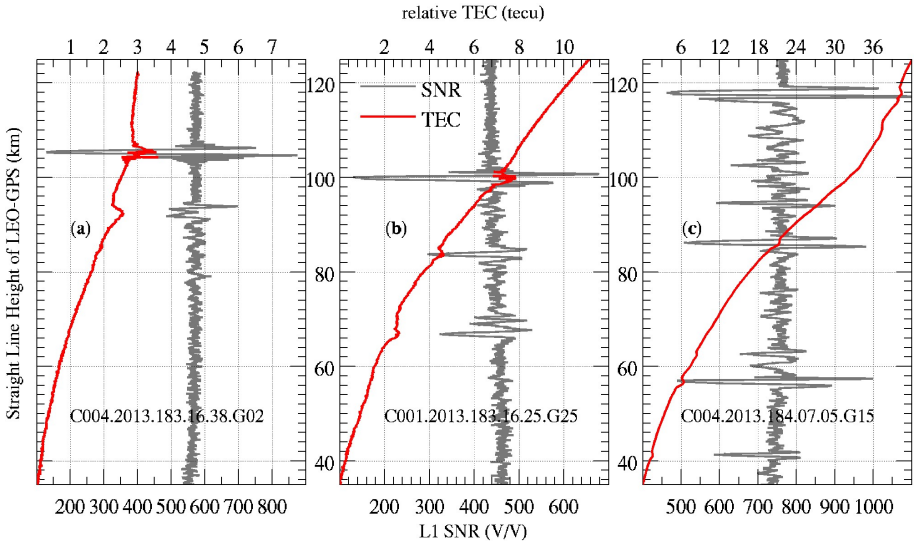

Figure 2. Selected examples of 2 **(a)**, 3 **(b)**, and multiple (**c**, 7 over here) peaks in the L1 SNR and relative slant TEC vs. straight line height observed by COSMIC satellites.

AMTD
7, 9203–9236, 2014

Case study on complex sporadic E layers observed by GPS radio occultations

X. Yue et al.

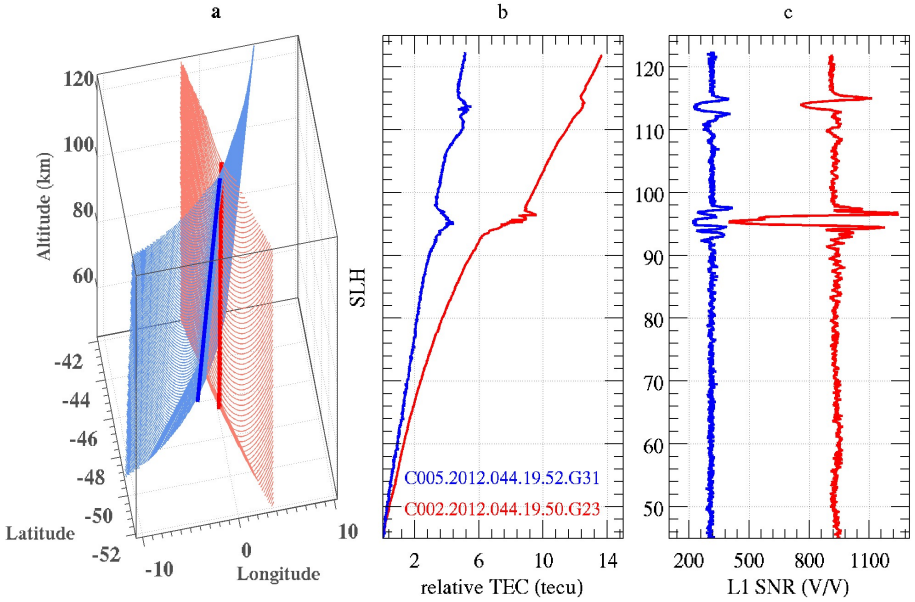

Figure 3. Two co-located RO events, which present 2 peaks in either relative TEC or L1 SNR vs. straight line height, observed by different COSMIC LEO satellites at the same time during 2012.044: **(a)** occultation plane and corresponding tangent points; **(b)** relative slant TEC vs. straight line height (SLH); **(c)** L1 SNR vs. straight line height. Color blue and red represent two RO events, respectively.

AMTD
7, 9203–9236, 2014

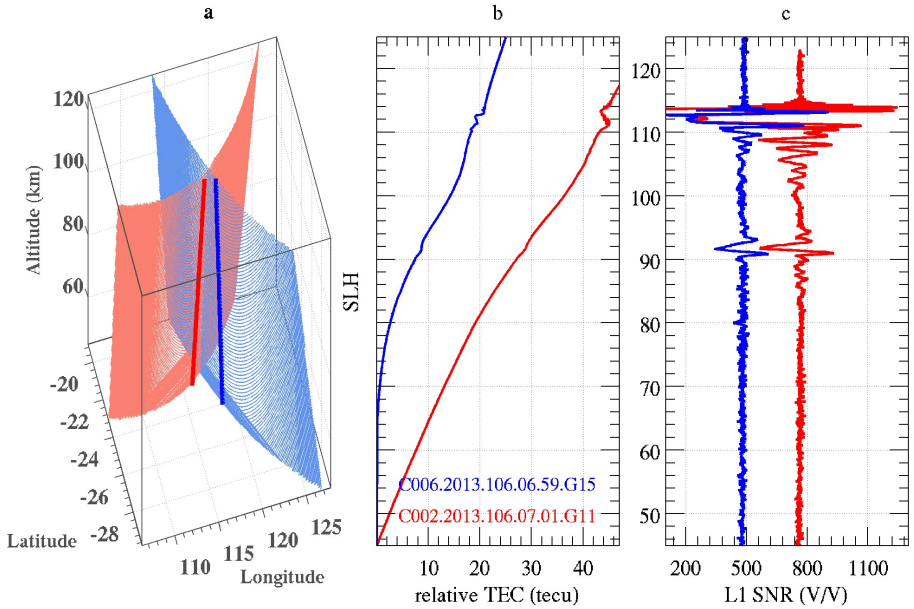

Figure 4. The same as Fig. 3, but for another case during 2013.106.

AMTD
7, 9203–9236, 2014

Case study on complex sporadic E layers observed by GPS radio occultations

X. Yue et al.

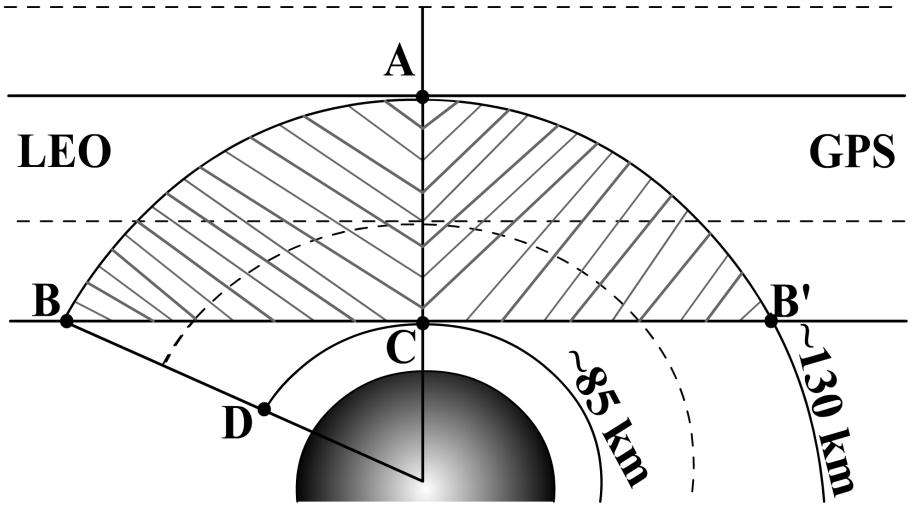

Figure 5. The Es Occurrence Area (EOA) is defined by the shadow area in the picture.

AMTD
7, 9203–9236, 2014

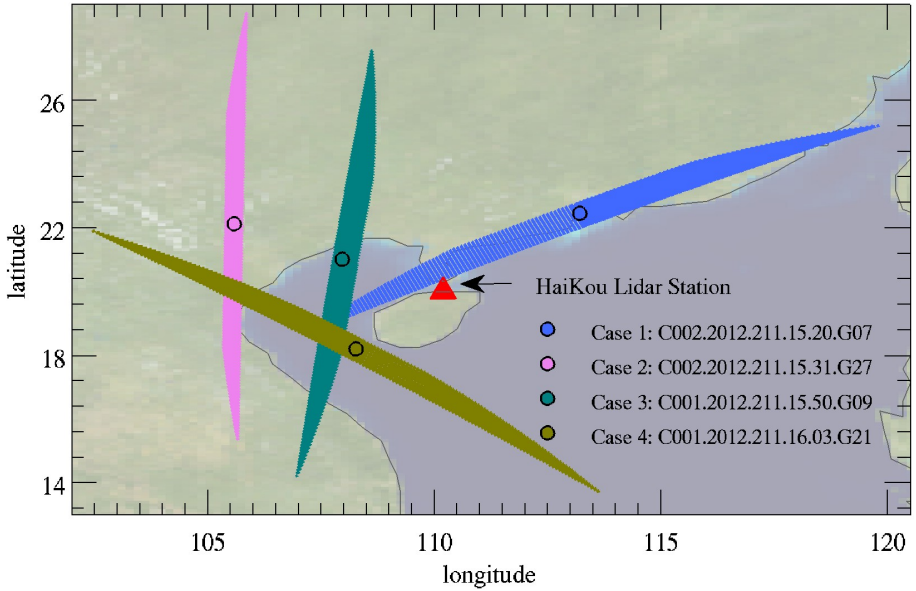

Figure 6. The red triangle represents the location of Hai Kou Lidar station over China. The shadow area shows the Es Occurrence Area (EOA) for the 4 co-located RO events observed by COSMIC and represented by 4 colors. The location of 100 km altitude of straight line is embedded by the circle.

AMTD
7, 9203–9236, 2014

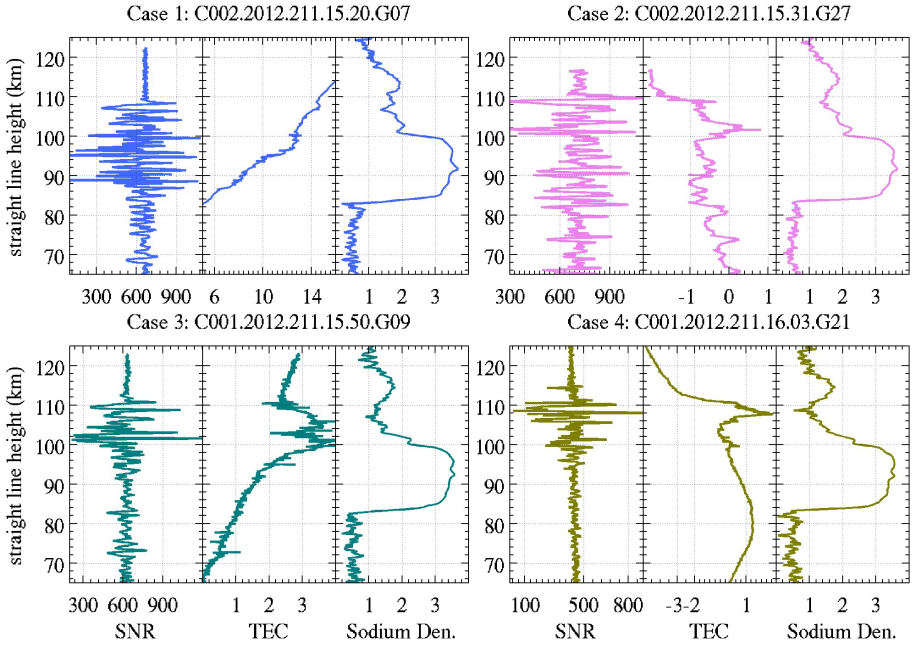

Figure 7. Altitude variations of L1 SNR and relative slant TEC of RO event and Na density of Lidar observations corresponding to the 4 cases shown in Fig. 6. The unit of Na density is cm^{-3} and has been taken logarithmic in the plots.

AMTD
7, 9203–9236, 2014

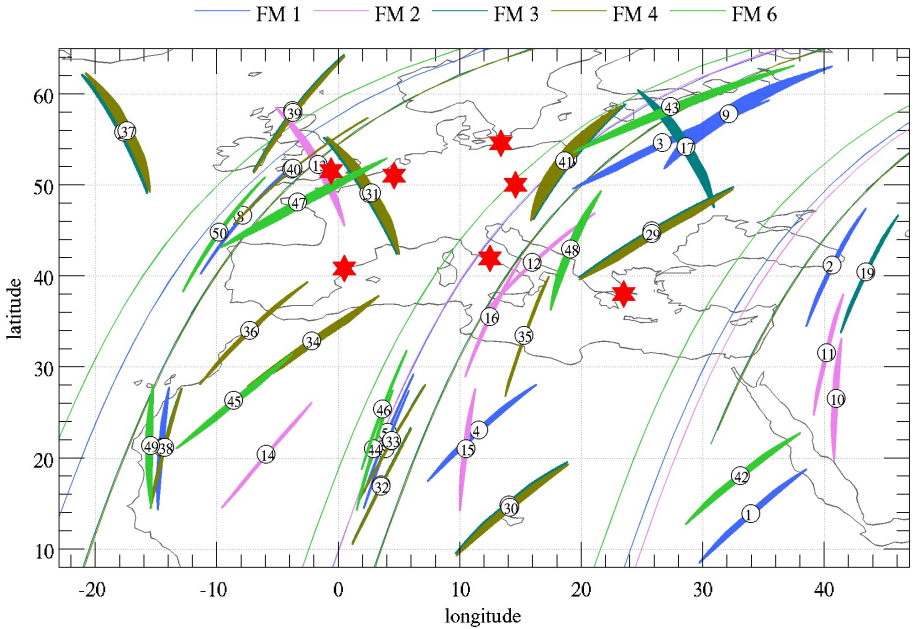

Figure 8. Longitude and latitude distributions of the Es Occurrence Area (EOA) of 50 RO events observed by COSMIC during 2006.294 11:00–15:00 UT over and surrounding Europe region. The circle on each EOA is the corresponding tangent point over 100 km altitude with the case serial number embedded. The light lines are the orbits of COSMIC LEO satellites during this time interval. Different colors represent different COSMIC FM satellites. The red stars show the location of 7 used Ionosondes.

AMTD
7, 9203–9236, 2014

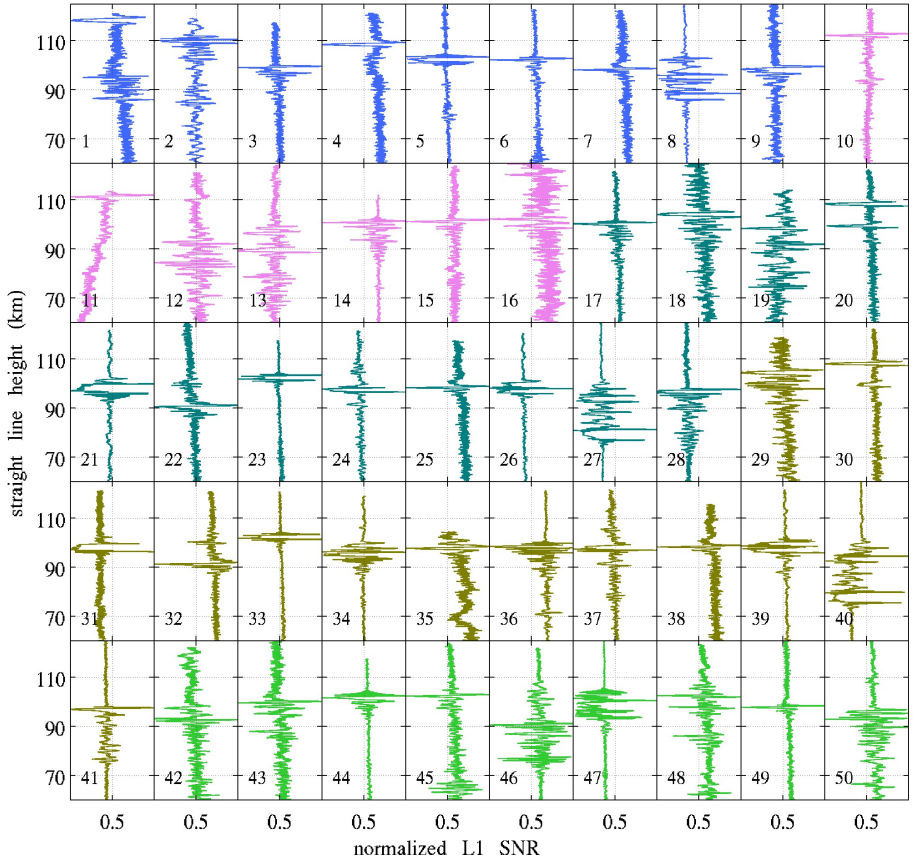

Figure 9. Straight line height variations of the normalized L1 SNR for the 50 COSMIC RO events shown in Fig. 8. Different colors represent different LEO satellites.

AMTD
7, 9203–9236, 2014

Case study on complex sporadic E layers observed by GPS radio occultations

X. Yue et al.

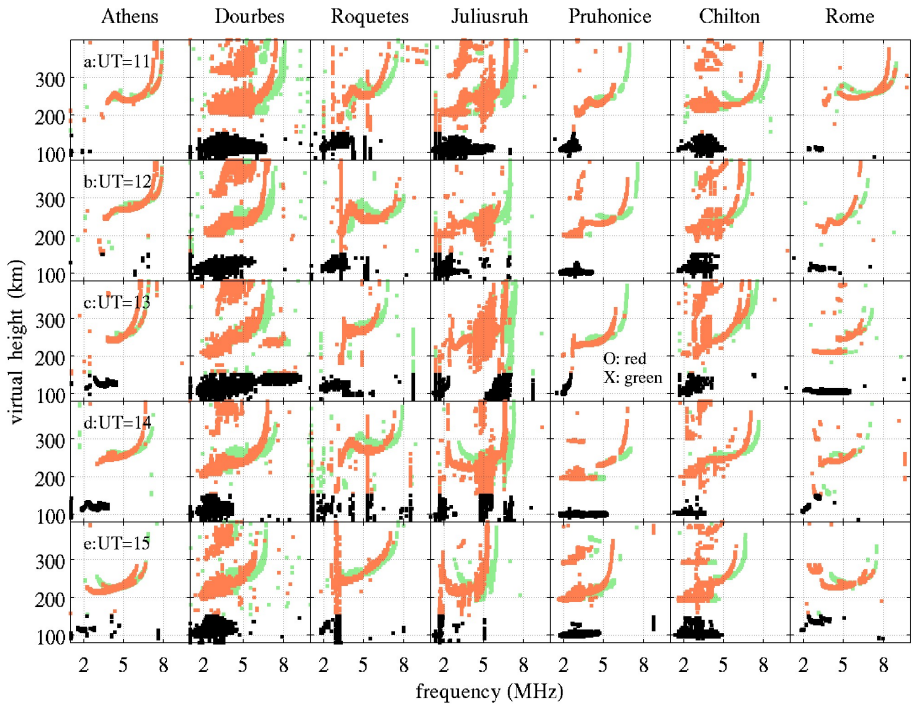

Figure 10. Raw ionogram: graph of the virtual height plotted against frequency. From the left to the right are for 7 ionosondes with the name on the top. Panels a to e are for university times of 11 to 15 with 1 h interval during 2006.294. Ordinary and extraordinary returned waves are represented by the red and green dots, respectively. The wave traces below ~ 150 km are given by the black dots to highlight the occurrence of sporadic E layer.

AMTD
7, 9203–9236, 2014

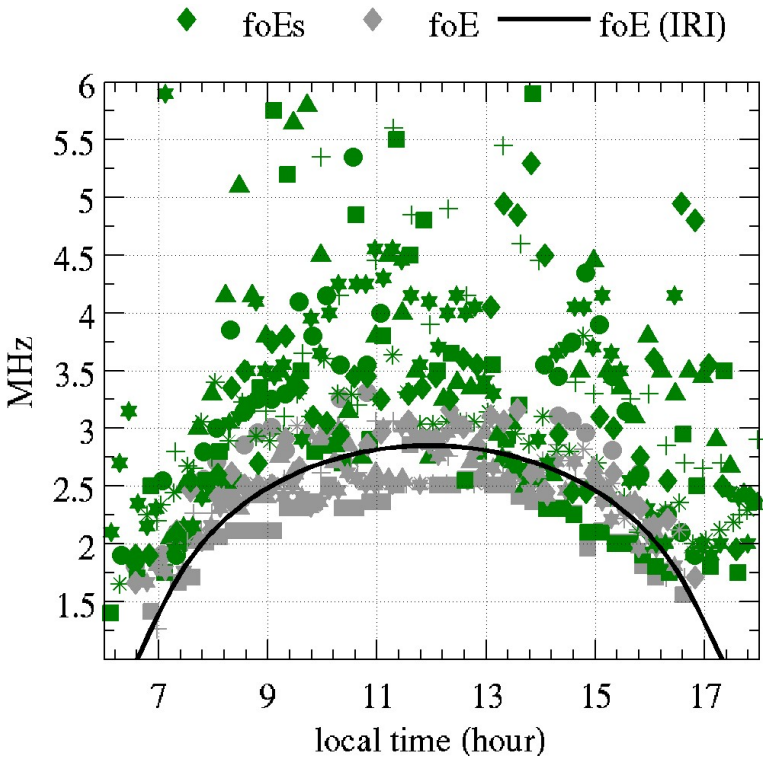

Figure 11. Local time variation of the sporadi E layer critical frequency (foEs, green) and the E layer critical frequency (foE, grey) observed by 7 selected ionosondes and the corresponding IRI modeled foE results (black line) during 2006.294. The results of different ionosondes are distinguished by the dot shape. The IRI model results are corresponding to the mean latitude and longitude of 7 ionosonde stations.

AMTD
7, 9203–9236, 2014